Structure of Semicrystalline Poly[bis(phenoxy)phosphazene] As Studied by ^{31}P Spectral Spin Diffusion

K. Takegoshi, Isao Tanaka, and Kunio Hikichi*

Department of Polymer Science, Faculty of Science, Hokkaido University, Sapporo 060, Japan

Shiro Higashida

Advanced Material Department, Nippon Soda Company, Ltd., Ichihara 290, Japan

Received November 8, 1991

ABSTRACT: Despite the single ^{31}P peak observed in solution, high-resolution solid-state ^{31}P NMR spectra of poly[bis(phenoxy)phosphazene] (PBPP) consist of two well-resolved peaks, whose intensities and positions show temperature dependence. Taking into account different characteristic spin dynamics, these two peaks are attributed to crystalline and amorphous parts of PBPP. It is shown that there exists a moderately fast spin diffusion between the two ^{31}P peaks. A close examination of the mixing-time dependence of the cross-peak intensity indicates an existence of the interface phase. The present experiments enable us to determine the temperature dependence of the ratio of amorphous, interface, and crystalline phases in the PBPP sample. Furthermore, the observed temperature dependence of the ^{13}C line widths of the side-chain group is analyzed, and the activation parameters of motion of the phenoxy group about its P–O bond are determined.

1. Introduction

Semicrystalline polymers consist of mainly two phases: a crystalline phase and an amorphous phase. High-resolution solid-state NMR has been one of the most useful methods in the investigation of phase structure in semicrystalline polymers.[1] In this work, we have studied poly[bis(phenoxy)phosphazene] (PBPP)

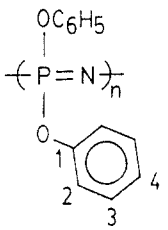

because this is a well-established semicrystalline polymer; its morphology has been extensively studied by X-ray and electron diffraction,[2] thermal analysis,[3] and transmitted light intensity methods.[4]

The main chain of polyphosphazenes is composed of an –N=P– sequence. Polyphosphazenes show three characteristic thermal transitions: (1) the glass transition, T_g, (2) the thermotropic transition at $T(1)$, and (3) the melting transition at T_m. A number of techniques have been applied to study the morphology of semicrystalline polyphosphazenes. The recent ^{31}P NMR study has shown that the ^{31}P signal from the crystalline phase disappears at the thermotropic transition temperature $T(1)$.[5] Furthermore, it was deduced by analyzing ^1H NMR free induction decay signals that a fraction of the Gaussian component decreases with increasing temperature up to its $T(1)$ of Ca. 403 K in parallel with the increase of the fraction of the Weibull component.[6] These two components were attributed, respectively, to the crystalline and the amorphous phases. It is, therefore, important to investigate how the crystalline phase transforms to the amorphous phase at temperatures between T_g and $T(1)$.

In this work, we apply high-resolution solid-state ^{31}P NMR techniques to investigate the structure of poly[bis(phenoxy)phosphazene] (PBPP) at temperatures between T_g and $T(1)$. We show that in this temperature range PBPP consists mainly of three phases: (i) crystalline, (ii) amorphous, and (iii) interface. The existence of the interface phase is demonstrated by spin-diffusion experiments, and the temperature dependence of these compositions is also demonstrated.

In addition, the temperature dependence of the ^{13}C line width of the side-chain phenoxy group is analyzed, and the activation parameters of motion of the phenoxy group about the P–O bond are determined.

2. Experimental Section

2.1. Samples. The poly[bis(phenoxy)phosphazene] used in this study is a commercial PLP-210 from Nippon Soda Co.; its weight-average molecular weight M_w is approximately 200 000 and T_g is approximately 265 K. Two samples were prepared by (1) casting a 5 wt % tetrahydrofuran (THF) solution and (2) precipitation from a 5 wt % THF solution in a large excess of hexane at room temperature. Both samples were dried under reduced pressure at 330 K for several days and heat-treated for 3 h at 393 K, i.e., just below or at the $T(1)$ of this PBPP, and gradually cooled to room temperature (the initial cooling rate is 1 K/min). The sample without such heat treatment showed a marked thermal hysteresis in the ^{31}P spectra. In this work, we mainly describe the results of the cast sample unless otherwise indicated.

Figure 1 shows the differential scanning calorimetry (DSC) curve of the cast sample, showing the glass transition at about 265 K and the thermotropic transition at about 408 K. The DSC curve was obtained using a Mettler DSC20 with a heating rate of 10 K/min.

2.2. X-ray Diffraction Measurements. X-ray diffraction measurements were made using a MAC Science DIP100 diffractometer equipped with an automated diffraction data collection system with an imaging plate.[7] Cu Kα radiation filtered by a graphite monochromator was used at 50 kV.

2.3. NMR Measurements. Both ^{31}P and ^{13}C NMR measurements were carried out on a JEOL JNM-GX270 spectrometer operating at frequencies of 109 MHz for ^{31}P, 67 MHz for ^{13}C, and 270 MHz for ^1H. The high-resolution solid-state NMR spectra were obtained by the combined use[8] of high-power proton decoupling (DD)[9] and magic-angle sample spinning (MAS).[10] The radio-frequency (rf) field strengths for ^1H, ^{31}P, and ^{13}C were about 55.6 kHz. The ^1H decoupling frequency was chosen to be 7 ppm downfield from $(CH_3)_4Si$ (TMS) for efficient decoupling of the phenoxy protons.[11] A double-bearing aluminum oxide rotor was used at a spinning frequency of 6 kHz at temperatures above 310

0024-9297/92/2225-3392$03.00/0

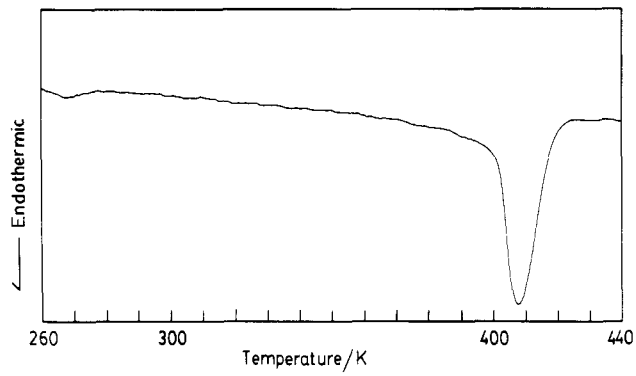

Figure 1. DSC curve for the PBPP heat treatment described in the text. The heating rate is 10 K/min.

K and in most cases of 5.6 kHz below 310 K. The setting of the magic angle was monitored by the ^{79}Br NMR spectrum of KBr incorporated in the rotor.[12] The ^{31}P chemical shifts were calibrated in ppm relative to 85% H_3PO_4 as an external reference standard. The ^{13}C chemical shifts were calibrated in ppm relative to TMS by taking the methine carbon resonance of solid adamantane (29.50 ppm) as an external reference standard. Variable-temperature measurements were accomplished using a JEOL MVT temperature controller. Temperature calibration was done as described elsewhere.[13] Signal accumulation was normally started 20 min after the desired temperature was reached.

The contact time for the cross-polarization signal enhancement[14] was 2 ms, and the repetition time of accumulation was 4 s. When the frequency of molecular motion is close to the proton rf strength, the motional modulation of a dipolar interaction reduces the efficiency of cross-polarization; the conventional cross-polarization method does not give a good signal-to-noise ratio. In such a case and also when accurate relative intensity is required, we adopted the conventional 90° pulse method of a typical repetition time of 70 s with high-power proton decoupling.

3. Results and Discussion

3.1. Crystallinity and Morphology. The X-ray diffraction experiments of both samples gave similar patterns consisting of a broad amorphous band and some sharp reflections. The cast film gave a sharp X-ray pattern and narrow ^{31}P NMR signals as compared to the precipitated one, indicating that a variation of the local conformations of PBPP is less for the former. The observed *d*-spacings are 11.2, 10.1, 8.4, 6.9, 5.0, 4.6, and 4.2 Å and are in good agreement with the results of the sample reported earlier.[2b] The degree of crystallinity was roughly estimated to be ca. 60% by comparing the area of the distinct crystalline peaks and that of the broad amorphous halos.[15] The estimated degree of crystallinity is consistent with those observed by solid-state ^{31}P NMR described below.

3.2. ^{31}P Spectra. This PBPP sample gives one sharp ^{31}P signal at −18 ppm in THF, indicating that the PBPP is linear (no significant branching exists).[16] On the other hand, in the solid state, two well-resolved signals are observed at around −10 and −20 ppm. A small peak at 9 ppm is from an unknown impurity; this disappears in the precipitated sample. Parts a–c of Figure 2 show typical ^{31}P MAS spectra of PBPP at three representative temperatures: (a) 272, (b) 339, and (c) 394 K. Similarly to the recent ^{31}P studies on other polyphosphazenes,[5] the relative intensity of the low-field peak at −10 ppm increases with decreasing temperature. Since the low-field peak shows a non-Lorentzian line shape, the intensity of the high-field peak was determined by fitting to a Lorentzian line shape and that of the low-field peak was estimated from the line shape after subtraction of the fitted high-field peak from the experimental line shape. Figure 3 shows the temperature dependence of the relative intensities of the low- and high-field peaks. Below 290 K, the high-field peak becomes too broad to deduce a correct intensity. We found that when the cross-polarization is applied, the relative intensity of the high-field peak at −20 ppm becomes smaller and that the apparent spin–lattice relaxation time of the high-field peak (4.9 at 317 K) is shorter than that of the low-field peak (15.2 s). Furthermore, the line shape of the high-field peak is found to be well described by a Lorentzian function, but the low-field peak is not. These results indicate that the low-field peak arises from polyphosphazene molecules in less mobile parts and the high-field peak from mobile parts. As shown by the X-ray diffraction experiments, there exist the crystalline phase and the amorphous phase. In reference to the earlier studies on other polyphosphazenes,[5] we attribute the low-field ^{31}P peak to the crystalline and the high-field one to the amorphous. It is shown that, even at the highest temperature of 393 K attainable to our probe,

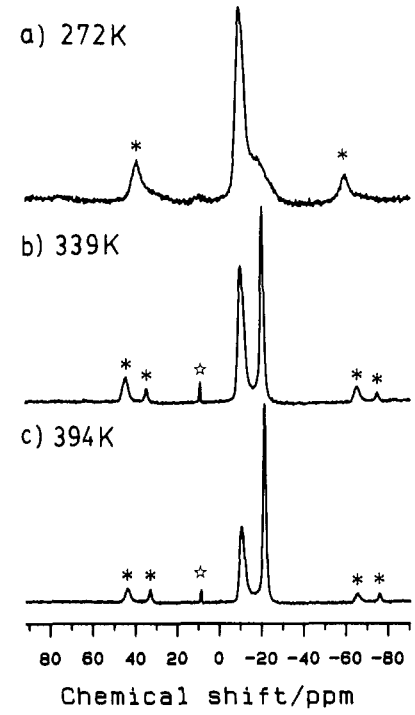

Figure 2. Solid-state ^{31}P MAS NMR spectra for PBPP at (a) 272 K, (b) 339 K, and (c) 394 K obtained by a 90° pulse with a repetition of 70 s. The peaks marked with asterisks are spinning side bands, and the peak marked with a star is from an unknown impurity.

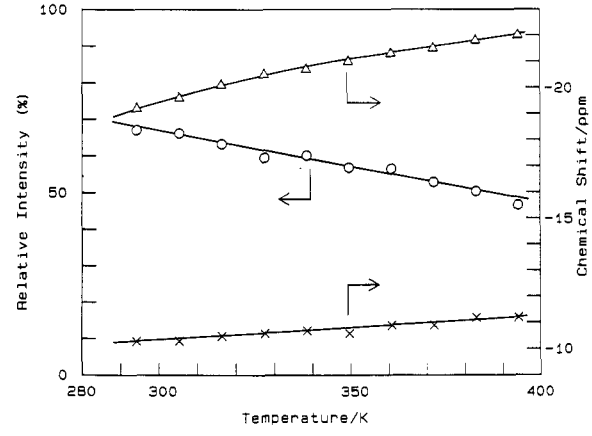

Figure 3. Temperature dependence of the relative intensity of the crystalline peak (○) and of the isotropic chemical shift of the crystalline peak (×) and the amorphous peak (△). The solid lines are to guide the reader's eyes.

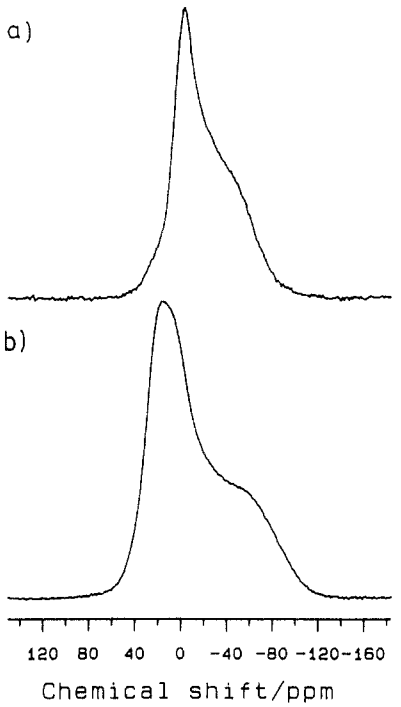

Figure 4. Solid-state powder ^{31}P NMR spectra of (a) the amorphous phase and (b) the crystalline phase.

there still exists a crystalline phase composing 46.5% of the sample. The ^{31}P chemical shifts also show the temperature dependence and are depicted in Figure 3. The amorphous peak is found to show a stronger dependence on the temperature. Similar results are obtained for the precipitated sample, although the amount of the crystalline phase is rather small.

The different spin dynamics of ^{31}P between the crystalline and amorphous phases enable us to observe the ^{31}P powder line shape of each phase (Figure 4). The powder line shape of the crystalline phase was obtained at room temperature by employing the cross-polarization enhancement technique with a short mixing time of 500 μs. The line shape of the amorphous phase was obtained by the delayed-decoupling pulse sequence[17] with a short repetition time of 1 s; the proton decoupling irradiation was turned off after the ^{31}P 90° pulse for a period of 100 μs. Although not perfect, the selectivity is good enough to show the powder line shapes for both phases. The line shapes of both phases show a so-called axially symmetric powder pattern; the components of the chemical shift tensor are found to be $\sigma_{11} = \sigma_{22} = 18$ and $\sigma_{33} = -65$ ppm for the crystalline and $\sigma_{11} = \sigma_{22} = 0$ and $\sigma_{33} = -55$ ppm for the amorphous. The isotropic chemical shifts δ calculated from the tensor components ($\delta = (\sigma_{11} + \sigma_{22} + \sigma_{33})/3$) are −10 and −18 ppm for the crystalline and amorphous phases, respectively; they are in good agreement with those observed by the MAS experiments.

It is worth noting that the shielding anisotropy for the crystalline part is larger than that of the amorphous fraction. Chain motion in the amorphous phase leads to a partial averaging of the shielding tensor. The observed axial symmetry of the shielding tensor may indicate that the π electrons in the P=N bond are delocalized and that the local distribution of electrons around the ^{31}P spin becomes axially symmetric. The observed large differences of the chemical shift values of ^{31}P in the crystalline and the amorphous phases may be ascribed to the different coherent lengths of the delocalized electrons. In the crystalline phase, π electrons are more widely distributed over the ordered P–N chain. In the amorphous phase, however, such delocalization may be confined to a smaller range because of the disordered chain conformation.

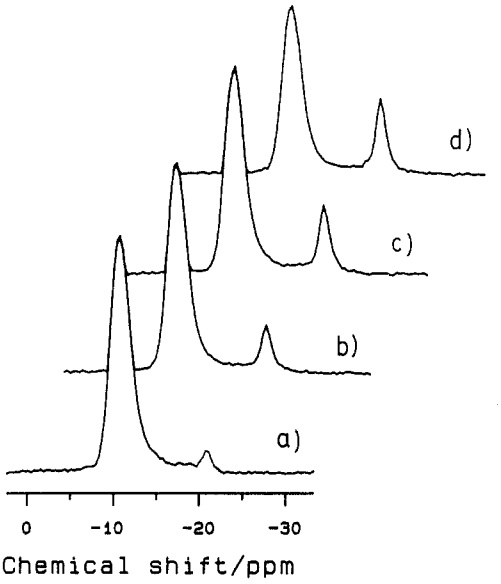

Figure 5. 1D-exchange ^{31}P NMR spectra of PBPP with mixing times of (a) 0.2, (b) 1, (c) 2, and (d) 4 s.

3.3. Spectral Spin Diffusion and Phase Structure. To obtain more detailed information as to how the amorphous–crystalline phases are interacting with each other, we have attempted a one-dimensional (1D)-exchange NMR experiment for the two well-resolved ^{31}P peaks. The 1D-exchange NMR technique applied here is described in detail in ref 18. The conventional pulse sequence used for the two-dimensional (2D)-exchange NMR experiment of a dilute spin in solids[19] is employed. The ^{31}P transmitter frequency is set to the resonance frequency of one of the two ^{31}P and the evolution time to satisfy $t_1 = 1/(4\Delta)$ where Δ is the off-resonance frequency in hertz of the other ^{31}P signal. By appropriate phase cycling, one can cancel the magnetization *recovered* by the spin–lattice relaxation time. The resulting 1D-exchange NMR spectrum corresponds exactly to a slice of a 2D-exchange NMR spectrum which passes through both the diagonal peak and the cross peak.

Figure 5 shows the 1D-exchange NMR spectra at 361 K at a mixing time τ of (a) 0.2, (b) 1, (c) 2, and (d) 4 s. Here, the transmitter frequency is on-resonance at the crystalline signal (the diagonal peak). The signal which appears at the amorphous position is the cross peak. The appearance of the cross peak obviously indicates that an exchange process takes place between the crystalline and the amorphous phases. Figure 5 shows the mixing-time dependence of the ratio of the cross and the diagonal peaks observed at 317 and 361 K.

A simple analysis of the mixing-time dependence of the cross/diagonal peaks was done on the basis of equations describing a two-site exchange, where a spin experiences two different chemical shifts during the t_1 period. The normalized magnetizations corresponding to a diagonal peak M_D and a cross peak M_C observed after the mixing time τ can be derived as[20]

$$M_C = \chi_D\chi_C(k/D)\exp(-\sigma\tau)\sinh(D\tau) \quad (1)$$

and

$$M_D = \chi_D\exp(-\sigma\tau)[\cosh(D\tau) - (\delta/D)\sinh(D\tau)] \quad (2)$$

with

$$D = (\delta^2 + \chi_D\chi_C k)$$

$$\delta = (R_{DD} - R_{CC})/2$$

$$\sigma = (R_{DD} + R_{CC})/2$$

$$R_{DD} = R_{1D} + \chi_C k$$

and

$$R_{CC} = R_{1C} + \chi_D k \quad (3)$$

Here, χ_D and χ_C denote the mole fractions of the diagonal peak and the cross peak ($\chi_C + \chi_D = 1$), respectively, k denotes the rate of exchange, and R_{1D} and R_{1C} are the spin–lattice relaxation rates for the diagonal peak and the cross peak, respectively.

The spin–lattice relaxation rates for the crystalline peak R_{1X} and for the amorphous peak R_{1A} were determined from the initial slope of the recovery curve observed by the inversion–recovery experiment. Observed values are 0.065 s^{-1} at 317 K and 0.079 s^{-1} at 361 K for $R_{1D} = R_{1X}$ and 0.20 s^{-1} at 317 K and 0.25 s^{-1} at 361 K for $R_{1C} = R_{1A}$. By taking the fraction of the crystalline phase χ_X (=χ_D) and k as two adjustable parameters, we fit the experimental data of the cross/diagonal ratio to eqs 1–3. The least-squares fitted parameters obtained are listed in Table I, and the "best fit" calculated lines are depicted as solid lines in Figure 6. It was found that the simple two-site model describes the 1D-exchange experiments satisfactorily.

The exchange rate is found to be temperature-independent. This means that the exchange is not a motional exchange but is caused by the spin-diffusion mechanism driven by the homonuclear ^{31}P–^{31}P dipole–dipole interaction. The longitudinal magnetization of the whole crystalline phase stored along the static field by the above-mentioned procedure is transferred to ^{31}P spins in the amorphous phase by mutual flip–flop motions of the pair of ^{31}P spins in the two phases.

The intense cross peak shows that a large fraction of the ^{31}P nuclei in the amorphous phase do participate in the spin diffusion. If only ^{31}P nuclei near the surface of the crystalline phase are involved, the resulting cross peak should be much smaller. However, the observed fraction of the crystalline phase χ_D in Table I is larger or that of the amorphous phase χ_C is smaller than that estimated from the signal intensity (Figure 3) at both temperatures. This indicates that not the whole amorphous phase is interacting with the crystalline phase; only a part of the amorphous phase is dipolar-coupled with the crystalline phase to give rise to the spin diffusion. This result suggests that (I) the presence of a phase whose spin dynamics is rather different from the remaining amorphous phase or that (II) the spin diffusion occurs only to such an extent for the current mixing time and the relaxation times. We shall tentatively call this part the interface phase. The amount of the interface phase can be calculated from the observed χ values at two temperatures given in Table I. The results are schematically shown in Figure 7.

To examine the above possibilities, the experiment of backward spin diffusion from the interface/amorphous peak to the crystalline peak was also performed at 317 K in which the transmitter frequency is chosen to be on-resonance at the high-field peak. The observed mixing-time dependence of the cross/diagonal (crystalline/amorphous) ratio is shown in Figure 8. The possibility of (II) is negated, since for such a model (II) eqs 1–3 should also be applicable. However, we could not find a good

Table I
Best Fit Parameters to the Cross/Diagonal Ratio in 1D-Exchange NMR[a]

temp/K	χ_D	k/s^{-1}
317	0.283 ± 0.008	0.62 ± 0.27
361	0.270 ± 0.003	0.61 ± 0.10

[a] Error is 2.5σ.

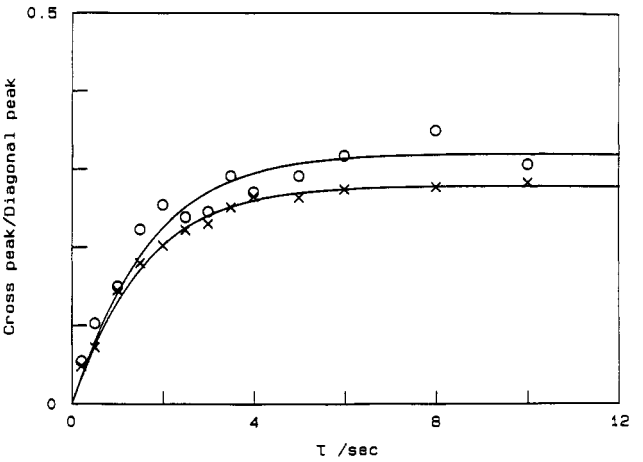

Figure 6. Mixing-time dependence of the cross/diagonal ratio of crystalline to amorphous 1D-exchange NMR. The solid curves through the data points are "best fits" described by the parameters in Table I.

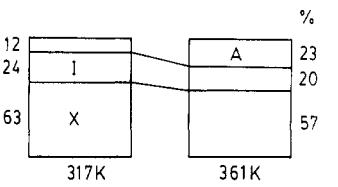

Figure 7. Schematical drawing of the phase composition of PBPP at (a) 317 and (b) 361 K. The letters A, I, and X denote the amorphous, the interface, and the crystalline phases, respectively.

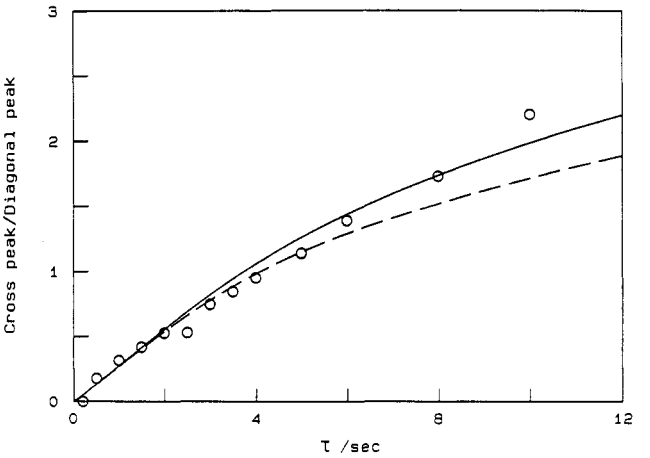

Figure 8. Mixing-time dependence of the cross/diagonal ratio of amorphous to crystalline 1D-exchange NMR. The dotted and the solid curves are the calculated ones with parameters in Table I and eq 4. The dotted line assumes the identical relaxation rate for the interface and the amorphous phases, and the solid line assumes a slightly faster rate for the amorphous phase.

agreement with the backward spin-diffusion data. For the model (I), we treated contributions of the magnetizations in the amorphous phase as follows:

$$\text{ratio} = M_C/(M_D + \chi_A \exp(-R_{1A}\tau)) \quad (4)$$

Here, the second term in the denominator is included to describe contributions of the decaying magnetization of

the amorphous phase during the mixing time. R_{1A} is the relaxation rate, and χ_A is the fraction of the amorphous phase. For the calculation of M_C and M_D from eqs 1–3, we adopt the fractions depicted in Figure 7 ($\chi_C = 0.63$, $\chi_D = 0.24$, and $\chi_A = 0.12$), the observed relaxation rates of $R_{1C} = 0.065$, $R_{1D} = 0.20$, and $R_{1A} = 0.20\ s^{-1}$, and the spin-diffusion rate of $k = 0.62\ s^{-1}$. As shown by the dotted line in Figure 8, the best fit parameters for the crystalline-to-interface diffusion can successfully realize the initial region of the backward spin diffusion. At longer mixing times, the discrepancy becomes apparent. The fitting becomes better if one adopts a slightly faster relaxation rate for the amorphous phase. The solid line in Figure 8 is the one calculated by using a value of $0.24\ s^{-1}$ for the relaxation rate of the amorphous phase, while keeping the observed relaxation rate ($0.20\ s^{-1}$) for the interface phase. The remaining discrepancy at longer mixing times may be due to the very slow spin-diffusion effects from the amorphous to the interface phase, which becomes apparent in this time region.

The agreement between the three-phases model (I) and the backward spin-diffusion experiments is satisfactory. In particular, an overall fitting is achieved using the parameters deduced from the forward spin-diffusion experiment. These results show that the ^{31}P spin-diffusion occurs in both the crystalline phase and the interface phase but not in the amorphous phase. The ^{31}P spins in PBPP are classified into three kinds with respect to the spin diffusion.

It is somewhat surprising that the simple two-site model (eqs 1–3) can describe complex spin-diffusion processes within a semicrystalline polymer. A physically more realistic model should include two interphase spin-diffusion processes occurring between crystalline and interface phases and between interface and amorphous phases and three intraphase spin-diffusion processes occurring within each phase. Furthermore, the interphase spin diffusion is effective at the surface region of each phase, and its efficiency decreases gradually with increasing inward distance from the surface. Hence, the spin-diffusion rate should have a distribution. Since experimental results could be satisfactorily fitted to the simple two-site model, it seems that there are several mechanisms acting to reduce the more complicated model to the simple two-site with a single spin-diffusion rate constant.

First, the ^{31}P–^{31}P dipolar interaction between the ^{31}P nuclei in the amorphous and the interface phases should be reduced substantially by molecular motion. Thus, it is reasonable to assume that the spin diffusion between the interface and the amorphous phases is much slower than that between the interface and the crystalline phases; the ^{31}P nuclei are rigid at least in the crystalline phase. Thus, a major interphase spin-diffusion process is between the interface and the crystalline phases, the spin-diffusion processes including the amorphous phase can be neglected. As suggested above, a better agreement should be achieved, especially for the data shown in Figure 8, if we include such a slow spin diffusion. For the crystalline to the amorphous/interface spin-diffusion experiment (Figure 6), the interface/amorphous spin-diffusion is less prominent, because the initial longitudinal magnetizations of both phases are zero, and the difference in spin temperature[21] between the two phases is small during the diffusion experiments.

Second, it may be appropriate to assume that, because of its rigidity, its closeness, and a greater spectral overlap, the diffusion rate *within* the crystalline phase is much faster than those between different phases. The whole crystalline phase can be described by one spin temperature during the spin–diffusion process between different phases, and the change in polarization due to spin diffusion at the surface of the crystalline phase is transferred to the whole crystalline phase in a shorter time scale. The change is so fast that the whole crystalline phase behaves as a uniform spin during the spin-diffusion process. In the interface phase, it is also possible for layers relatively distant from the crystalline surface to participate in the spin diffusion. Here, we shall estimate the distance between the ^{31}P nuclei from the observed spin-diffusion rate.

The spin-diffusion rate k can be simply written as[22]

$$k = (\pi/2)\omega^2 F(0) \tag{5}$$

Here, $F(0)$ is the probability that the two spins have the same resonance frequency simultaneously. ω is the measure of the strength of the dipole interaction

$$\omega = \gamma^2\hbar/(2r^3)(3\cos^2\theta - 1) \tag{6}$$

where r is the distance between the two ^{31}P spins, and θ is the angle between the ^{31}P–^{31}P vector and the static magnetic field. A more detailed treatment of spectral spin diffusion under magic-angle spinning may be found in ref 23. To estimate the distance, we assume that $F(0)$ of PBPP is the same as that of $[(CH_3)_2NH_2]_8[P_2W_{17}O_{61}Zn(OH_2)]$, in which the spin-diffusion rate ($1.8\ s^{-1}$)[24] and internuclear distance are known.[25] Since the distance of the two ^{31}P in the latter compound is 3.9 Å, the distance in the PBPP is estimated to be 4.6 Å.

The distance is an average distance between the ^{31}P nuclei at the surface of the crystalline phase and its spin-diffusion partner in the interface phase. The short distance envisages us that the interface phase exists at the surface of the crystalline phase and its thickness is about 10 Å or that the spin diffusion within the interface phase is very fast. Thus, the spin-diffusion rate between the crystalline and the interface phases is determined by the ^{31}P nuclei at the very surface of the phases. In both cases, the distribution of the diffusion rate would be small. These allow us to describe the present spin-diffusion process as the two-site model.

The spin diffusion also affects the relaxation behavior of the interacting spins. It manifests itself as a nonexponential decay/recovery of the magnetization. In this sample, the observed recovery curves for both signals show slight nonexponential nature. This is a reason why we consider the initial slope as the relaxation rate. The relaxation decay curves were successfully analyzed using the parameters determined by the spin-diffusion experiments. The difference in mobility of the chain in the interface and the amorphous phases may reflect the different spin–lattice relaxation rates in both phases. In poly[bis(4-ethylphenoxy)phosphazene], it was suggested that the ^{31}P spectra consist of three peaks especially at lower temperatures.[5a] In this case, the three peaks from higher to lower field are assigned to the amorphous, the interface, and the crystalline phases, respectively. In PBPP, we could not find a distinct peak for the interface phase. Furthermore, a contact-time dependence of the ^{31}P signals was examined. We could not, however, find an apparent two-step contact-time dependence expected for the amorphous/interface peak. This insensitivity arises because the cross-polarization dynamics is also largely affected by the motional states of proton spins in both phases. The proton spins of PBPP exist only on the side-chain phenoxy group, and, as will be shown below, the

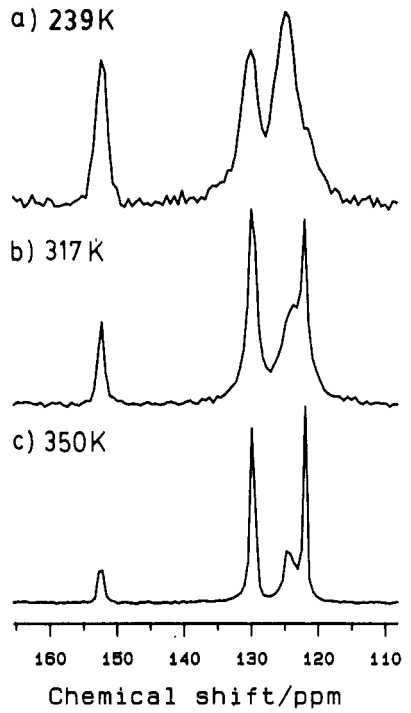

Figure 9. Solid-phase ^{13}C MAS NMR spectra of PBPP at (a) 239, (b) 317, and (c) 350 K. Spectrum a was obtained by the CP method, and spectra b and c were obtained by the 90° pulse method with a repetition time of 70 s.

side-chain motion is less sensitive to the difference in crystallinity.

As a summary, the crystalline phase is characterized as rigid and ordered, the interface phase as rather rigid and disordered, and the amorphous phase as mobile and disordered. The fraction of the interface phase is similar to those observed for polyethylene,[26] in which the crystalline, the interface, and the amorphous phases are characterized in terms of the chemical shift and spin–lattice and spin–spin relaxation times.

3.4. Side-Chain Motion. In addition to the results of the ^{31}P NMR study of the main chain, we describe a ^{13}C NMR study of the side-chain phenoxy group. Figure 9 shows ^{13}C spectra at three different temperatures. ^{13}C spectra consist of four peaks (Figure 9), which are assigned to C1 at 151.1 ppm, C2 at 120.7 ppm, C3 at 128.5 ppm, and C4 at 123.5 ppm with reference to the phenol and the biphenyl ether assignments.[27] Contrary to the expectation that the above-memtioned phase structures would also affect the ^{13}C spectra, neither apparent shifts due to the different crystallinity nor different spin dynamics are observed. We observe, however, an anomalous broadening for the C4 carbon signal. This broadening is attributable to a motional broadening[28] due to interference between the rotational motion about the P–O bond and the ^{1}H spin decoupling.

The observed spectra were fitted to the sum of Lorentzian line shapes to deduce the line widths. Figure 10 shows the temperature dependence of the line widths of the C3 and the C4 carbon signals. The solid line drawn through the data is the least-squares fit to the following empirical equation.[13]

$$\delta = \delta_0 + \delta_1(2/\pi)\arctan(\alpha(T_0 - T)) + \lambda M_2 J(\omega_1,\tau) \quad (7)$$

Here, the first term represents the intrinsic line width accounting for various *static* line-broadening mechanisms. The second term represents a normal motional-narrowing process, which we assume to have the arctan dependence on temperature. δ_1 is half of the line width due to the distribution of the isotropic chemical shifts, α describes the steepness of the dependence, and T_0 is a characteristic transition temperature. The third represents the interference term.[28] M_2 is the powder average of the second moment of the ^{13}C–^{1}H dipolar fields, and λ ($0 \le \lambda \le 1$) is the reduction factor of the second moment; for isotropic motion $\lambda = 1$. $J(\omega_1,\tau)$ is the spectral density of motion having the correlation time τ at the decoupling strength ω_1. This is the motional broadening term and has its maximum broadening at $\omega_1\tau = 1$ when τ is varied. For the CH carbon, the maximum broadening is calculated to be 1852 Hz for $\omega_1/2\pi$ of 55.6 kHz and r of 1.1 Å. A more detailed description of this equation is found in ref 13. The correlation time τ is assumed to have an Arrhenius dependence on temperature

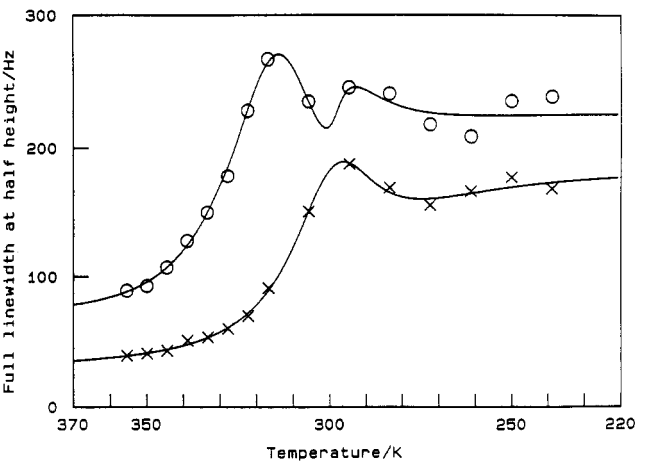

Figure 10. Temperature dependence of the full line width at half-height of the C3 (×) and the C4 (○) carbons of PBPP. The solid curves are best fit lines.

$$\tau = \tau_0 \exp(E_a/RT) \quad (8)$$

where E_a is the activation energy and τ_0 is the correlation time at infinite temperature. The observed line widths are least-squares fitted to eqs 7 and 8 by taking δ_0, δ_1, α, T_0, and λ in eq 7 and τ_0 and E_a in eq 8 as adjustable parameters. Error for each observed line width was assumed to be 10% of the line width.

The line width becomes temperature-independent at lower temperatures. The C3 line width (170 Hz) is less than that of C4 (230 Hz). Although the line-width data are rather scattered at these temperatures, these data are not very important for estimating the activation parameters. The reduction factor for C3 is smaller than that of C4. This indicates that the ^{1}H–^{13}C dipolar interaction for C3–H is averaged to a small value by the fast rotation of the phenoxy group about the O–C1 bond. Note that this motion does not affect the C4–H dipolar interaction. The further decrease of the dipolar interaction at $T_0 \sim 297$ K observed for both C4–H and C3–H suggests the onset of the motion about the O–P bond. The activation energy of this motion is found to be 17 ± 3 kcal/mol (error is 2.5σ).

4. Concluding Remarks

By examining the behavior of spin diffusion between different phases in a semicrystalline polymer, it is possible to investigate how these phases relate to each other. So far, most studies are concerned with the ^{1}H spin-diffusion effects on the ^{1}H relaxation times, mainly because other nuclei such as ^{13}C are too dilute to give rise to apparent spin-diffusion effects on its relaxation behavior. Such studies include direct examination[29] of ^{1}H T_2 and $T_{1\rho}$ and indirect examinations through ^{13}C spins.[1] Only a few

studies, including this work, have observed the spectral spin diffusion between different microphases directly by the exchange NMR techniques.[30] This may be due to difficulty in observing well-resolved lines. It should be mentioned here that the signal resolution for different phases is not a prerequisite for the 1D-exchange NMR experiment, even though signals from different phases do overlap with each other; if only their spin dynamics are different, in such cases of different spin–lattice relaxation rates and/or different cross-polarization efficiencies, one can discriminate magnetizations from different phases using some selective excitation methods; and a gradient of the spin temperature required for observing the spin diffusion can be established. An example of such selection of magnetization utilizing different spin dynamics is shown in Figure 4, where we observe ^{31}P powder patterns. Furthermore, indirect observation of a flip-flop motion of ^{1}H spins through ^{13}C spins[31] may be applicable.

Acknowledgment. We thank L. D. Ren and Professor S. Tokura for DSC measurements. Financial support for this work was provided by Grants-in-Aid of the Ministry of Education, Science, and Culture of Japan (01750815 and 02554014).

References and Notes

(1) For a review, see: Axelson, D. E. *High Resolution NMR Spectroscopy of Synthetic Polymers in Bulk*; Komoroski, R. A., Ed.; VCH: Deerfield Beach, FL, 1986; Chapter 5.
(2) (a) Kojima, M.; Magill, J. H. *Polymer* **1989**, *30*, 1856. (b) Masuko, T.; Sato, M.; Kojima, M.; Satake, S.; Magill, J. H. *Polym. Prepr. (Polym. Sci. Jpn., Polym. Symp.)* **1985**, *34*, 2109.
(3) (a) Kozmiski, S. J.; Harrison, I. R. *J. Appl. Polym. Sci.* **1982**, *27*, 1783. (b) Sun, D. S.; Magill, J. H. *Polymer* **1987**, *28*, 1243.
(4) Masuko, T.; Okuizumi, R.; Yonetake, K.; Magill, J. H. *Macromolecules* **1989**, *22*, 4636.
(5) (a) Tanaka, H.; Gomez, M. A.; Tonelli, A. E.; Chichester-Hicks, S. V.; Haddon, R. C. *Macromolecules* **1988**, *21*, 2301. (b) Tanaka, H.; Gomez, M. A.; Tonelli, A. E.; Chichester-Hicks, S. V.; Haddon, R. C. *Macromolecules* **1989**, *22*, 1031. (c) Young, S. G.; Magill, J. H. *Macromolecules* **1989**, *22*, 2549.
(6) (a) Sato, K.; Masuko, T. *Polym. Prepr. (Polym. Sci. Jpn., Polym. Symp.)* **1986**, *35*, 869. (b) Sato, K.; Masuko, T. *Polym. Commun.* **1986**, *27*, 299.
(7) Tanaka, I.; Yao, M.; Suzuki, M.; Hikichi, K.; Matsumoto, T.; Kozasa, M.; Katayama, C. *J. Appl. Cryst.* **1990**, *23*, 334.
(8) Schaefer, J.; Stejskal, E. O. *J. Am. Chem. Soc.* **1976**, *98*, 1031.
(9) Sarles, L. R.; Cotts, R. M. *Phys. Rev.* **1958**, *111*, 853.
(10) Andrew, E. R. *MTP Int. Rev. Sci., Phys. Chem. Ser. 2* **1975**, *4*, 173.
(11) Takegoshi, K.; McDowell, C. A. *J. Magn. Reson.* **1986**, *66*, 14.
(12) Frye, J. S.; Maciel, G. E. *J. Magn. Reson.* **1982**, *48*, 125.
(13) Takegoshi, K.; Hikichi, K. *J. Chem. Phys.* **1991**, *94*, 3200.
(14) (a) Hartmann, S. R.; Hahn, E. L. *Phys. Rev.* **1962**, *128*, 2042. (b) Pines, A.; Gibby, M. G.; Waugh, J. S. *J. Chem. Phys.* **1973**, *59*, 569.
(15) Nichols, J. B. *J. Appl. Phys.* **1954**, *25*, 840.
(16) Mujumdar, A. N.; Young, S. G.; Merker, R. L.; Magill, J. H. *Macromolecules* **1990**, *23*, 14.
(17) Opella, S. J.; Frey, M. H. *J. Am. Chem. Soc.* **1979**, *101*, 5854.
(18) Connor, C.; Naito, A.; Takegoshi, K.; McDowell, C. A. *J. Magn. Reson.* **1985**, *113*, 123.
(19) Szeverenyi, N. M.; Sullivan, M. J.; Maciel, G. E. *J. Magn. Reson.* **1982**, *47*, 462.
(20) Jeener, J.; Meier, B. H.; Bachmann, P.; Ernst, R. R. *J. Chem. Phys.* **1979**, *71*, 4546.
(21) Abragam, A. *The Principles of Nuclear Magnetism*; Clarendon: Oxford, U.K., 1961; Chapter V.
(22) Reference 21, p 138.
(23) Kubo, A.; McDowell, C. A. *J. Chem. Soc., Faraday Trans. 1* **1988**, *84*, 3713.
(24) Clayden, N. J. *J. Magn. Reson.* **1986**, *68*, 360.
(25) Dawson, B. *Acta Crystallogr.* **1953**, *6*, 113.
(26) Kitamaru, R.; Horii, F.; Murayama, K. *Macromolecules* **1986**, *19*, 636.
(27) Levy, G. C.; Lichter, R. L.; Nelson, G. L. *Carbon-13 Nuclear Magnetic Resonance Spectroscopy*, 2nd ed.; Wiley: New York, 1980.
(28) (a) VanderHart, D. L.; Earl, W. L.; Garroway, A. N. *J. Magn. Reson.* **1981**, *44*, 361. (b) Rothwell, W. P.; Waugh, J. S. *J. Chem. Phys.* **1981**, *74*, 2721.
(29) (a) Assink, R. A. *Macromolecules* **1978**, *11*, 1233. (b) Cheung, T. T. P.; Gerstein, B. C.; Ryan, L. M.; Taylor, R. E.; Dybowski, C. R. *J. Chem. Phys.* **1980**, *73*, 6059. (c) Cheung, T. T. P.; Gerstein, R. C. *J. Appl. Phys.* **1981**, *52*, 5517. (d) McBrierty, V. J.; Douglass, D. C. *J. Polym. Sci., Macromol. Rev.* **1981**, *16*, 295. (e) Cheung, T. T. P. *J. Chem. Phys.* **1982**, *76*, 1248. (f) Packer, K. J.; Pope, J. M.; Yeung, R. R.; Cudby, M. E. A. *J. Polym. Sci., Polym. Phys. Ed.* **1984**, *22*, 589. (g) Havens, J. R.; Vanderhart, D. L. *Macromolecules* **1985**, *18*, 1663.
(30) Axelson, D. E.; Mandelkern, L.; Popli, R.; Mathieu, P. *J. Polym. Sci., Polym. Phys. Ed.* **1983**, *21*, 2319.
(31) Takegoshi, K.; McDowell, C. A. *J. Chem. Phys.* **1986**, *84*, 2084.

Registry No. PLP-210, 124449-26-9.